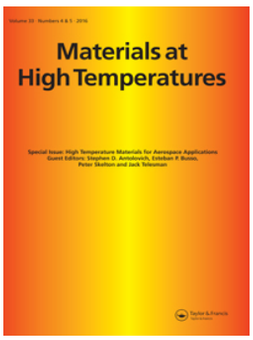

Materials at High Temperatures

ISSN: 0960-3409 (Print) 1878-6413 (Online) Journal homepage: http://www.tandfonline.com/loi/ymht20

Thermo-mechanical deformation evolution in polycrystalline Ni-based superalloys by a hierarchical crystal plasticity model

George R. Weber & Somnath Ghosh

To cite this article: George R. Weber & Somnath Ghosh (2016) Thermo-mechanical deformation evolution in polycrystalline Ni-based superalloys by a hierarchical crystal plasticity model, Materials at High Temperatures, 33:4-5, 401-411, DOI: 10.1080/09603409.2016.1190147

To link to this article: http://dx.doi.org/10.1080/09603409.2016.1190147

Thermo-mechanical deformation evolution in polycrystalline Ni-based superalloys by a hierarchical crystal plasticity model

George R. Weber and Somnath Ghosh*

A hierarchical plasticity constitutive model is employed to comprehend the fundamental relations between microstructural morphology, crystal orientations, deformation mechanisms and the mechanical response over a wide range of operating temperatures for polycrystalline nickel-based superalloys. A parametrically homogenised, crystal plasticity constitutive law accounting for the variation in the subgrain-scale $\gamma\gamma'$ morphology allows for efficient modelling at the polycrystalline scale with information from the lower scales. This framework incorporates the effects of non-Schmid mechanisms, anti-phase boundary shearing and geometric features of the $\gamma\gamma'$ substructure. A major outcome of this study is the observation that at elevated temperatures, a slip mode transition occurs from the octahedral slip systems to cube slip systems that induces a reversal of many critical mechanical properties. The polycrystalline microstructure is significantly weakened, and plastic deformation completely shifts to grains for which the orientation corresponds to the greatest resolved shear stress on cube slip systems.

Keywords: Crystal plasticity, Hierarchical model, Ni-based super alloys, Polycrystalline, Cube slip

Introduction

Nickel-based superalloys constitute a class of materials that have extensive applications in aerospace propulsion. Jet engine turbine components, such as blades and disks, rely heavily on their exceptional properties to withstand creep and fatigue in extreme thermal and corrosive environments. These superalloys are able to maintain their strength at a range of low to high temperatures, which allow engines to operate at high efficiency without mechanical failure. Large economic gains can be achieved by improving reliability and life of their aerospace applications through better predictability of relevant properties. Thermo-mechanical properties at continuum scales are highly influenced by the microstructure and microscale deformation mechanisms inherent to the material. Development of computational models at a hierarchy of spatial scales, incorporating appropriate scale-relevant mechanisms like dislocation mechanisms and morphology such as lattice orientations and statistical distributions of crystal and phase features, is critical to the prediction mechanical behaviour. Grain-scale crystal plasticity-based computational models have been developed in Refs. 1–6.

For Ni-based superalloys, much of the excellent mechanical behaviour can be attributed to the existence of a two-phase $\gamma\gamma'$ matrix–precipitate microstructure. The chemical composition varies with the specific superalloy, but in general, the γ matrix phase primarily consists of nickel with solid solutioning components, while the γ' precipitate phase is a coherent intermetallic Ni_3Al phase. The crystal structures of γ and γ' phases are FCC and $L1_2$, respectively. A multitude of physical phenomena are the result of the atomic structure of the γ' precipitate phase, and its presence in the γ matrix causes strengthening mechanisms for the two-phase system. In FCC and $L1_2$ crystal structures, dislocations have Burgers vectors with the same $\langle 1\ 0\ 1\rangle$ directions but different magnitudes. A full dislocation in the $L1_2$ structure must transverse twice the distance compared to that of FCC in order to maintain the ordered lattice, which creates many additional consequences for the dislocation core.

The effects of temperature on the mechanical response of Ni-based superalloys have been thoroughly investigated in the literature, and it has been demonstrated that the γ' phase is responsible for fundamental thermal aspects of plasticity in the material. Unlike most other metallic materials, $L1_2$ intermetallics are experimentally observed to exhibit an anomalous yield behaviour, in that the yield strength of the material increases with increase in temperature within a given temperature range.[7–13] In addition, tension–compression asymmetry of the yield strength is observed, depending on the loading orientation.[11,13,14] A quantitative description of dislocation core mechanisms has been provided to capture and explain these uncommon behaviours in the PPV models of[10,15,16], which can be rationalised by the consideration of two physical phenomena, Kear–Wilsdorf (KW) locks and cube slip. The PPV model and its variants are some of the most widely known and used models for $L1_2$ alloys. The benefit of their adoption is the ability to offer an explanation for an array of experimental results performed at many different mechanical and thermal conditions. While this is the most widely accepted explanation, there have been some reservations expressed against the model, e.g. in Refs. [17–19]. These authors have argued that the explanation is incomplete in the sense that the yield strength of superalloys starts increasing at temperatures even below 100 K, challenging the claim that

Departments of Civil, Mechanical, and Materials Science & Engineering, Johns Hopkins University, Baltimore, MD 21218, USA

*Corresponding author, email sghosh20@jhu.edu

Received 8 February 2016; accepted 8 May 2016
DOI 10.1080/09603409.2016.1190147

thermally activated mechanisms alone can fully describe the anomalous yield behaviour. Nevertheless, the PPV model is pursued in the present work due to its ability to capture a wide variety of micromechanical phenomena for superalloys.

In the $L1_2$ crystal structure, plasticity is carried by $a\langle 1\,0\,1\rangle$ superdislocations where a is the lattice parameter. In order to travel through the lattice structure of a $\langle 1\,1\,1\rangle$ plane, it is necessary for the dislocation to dissociate into two $\frac{a}{2}\langle 101\rangle$ superpartial dislocations separated by an anti-phase boundary (APB). It is generally energetically favourable for each $\frac{a}{2}\langle 101\rangle$ superpartial to extend further to create two $\frac{a}{6}\langle 112\rangle$ Shockley partials and a complex stacking fault. The fully extended superdislocation consisting of four Shockley partials, two complex stacking faults and an APB is now restricted to remain planar on an octahedral plane.[20] With screw dislocations of this type, cross slip to either an octahedral or cube plane becomes a possible mechanism if the leading superpartial undergoes constriction. In this event, cross slip is driven to favour cube slip planes by the anisotropy of the APB energy, i.e. lower APB energy on $\{001\}$ than on $\{111\}$.[9,20] However, a constricted superpartial typically travels only a small distance on a cube plane before redissociating back onto an octahedral plane, causing the full dislocation to become sessile.[15] This locked configuration of the superdislocation is denoted as KW lock.[21] The pinned dislocation segments of the KW lock serve as barriers to further dislocation motion and cause an overall hardening in the material. Since the superpartial constriction process is thermally activated, the occurrence of locked screw dislocations increases with temperature, which thereby explains the increase in yield strength with temperature. In addition, cross slip onto octahedral and cube planes can be promoted or impeded depending on whether the resolved shear stresses on the planes of interest act to extend or constrict the superpartials. This action confirms that the generation of KW locks depends on non-Schmid behaviour and leads to asymmetries between experimental tension and compression tests.

Additional microscale behaviour is observed by studying the effects of the $L1_2$ intermetallics as a γ' precipitate in a γ matrix. A primary mechanism of the yield behaviour of superalloys is APB shearing. Dislocations are driven by resolved shear stresses from the matrix phase through the precipitate in a dissociated form. As a dislocation from the γ phase penetrates into the γ' phase, it becomes a leading superpartial and leaves an APB in its wake. The APB is then removed as a second dislocation passes into the precipitate and acts as a trailing superpartial. Due to the additional energy barriers associated with this process, the presence of γ' precipitates provides significant obstacles for plasticity and, therefore, strengthens the overall material.

The development of constitutive models that can capture dominant micro-mechanisms of Ni-based superalloys must be put into a context that can be connected to higher length scales. A multi-scale framework has been developed to incorporate the effects of subgrain dislocation mechanisms in the $\gamma\gamma'$ phases into mechanical analyses at the polycrystalline scale in[5,6,22,23]. At the lowest scale, an explicit $\gamma\gamma'$ representative volume element (RVE) structure is deformed using a dislocation density-based crystal plasticity formulation under a range of loading and thermal conditions and with various $\gamma\gamma'$ morphologies.[5,6,22,24] With an understanding of the constitutive behaviour at the RVE scale, a homogenisation process is implemented to develop a single-crystal constitutive law accounting for the $\gamma\gamma'$ subgrain morphology in the form of parametrised hardening variables. This methodology permits computationally efficient polycrystalline simulations to be performed while retaining the important details of the mechanical response at the subgrain scale.

The objective of this paper is to apply the multi-scale framework to provide an understanding of the influence of temperature on the deformation behaviour of polycrystalline superalloys. There are inherent links between the thermal environment and microscale mechanical mechanisms such as activation of specific sets of slip systems undergoing dislocation motion, crystal loading orientations, non-Schmid yielding influenced by the $\gamma\gamma'$ substructure and local stress state development at hard and soft grains. The role of temperature is analysed in relation to these microstructural effects with the two-scale constitutive model accounting for subgrain behaviour over a wide range (300–1300 K) of isothermal simulations.

Constitutive model for single-crystal Ni-based superalloys

A homogenised framework has been constructed in[5,6,22] for Ni-based superalloys to enable a polycrystalline scale model to account for variations in the distributions of $\gamma\gamma'$ subgrain morphology, as shown in Fig. 1. This framework is implemented in the present study to enable polycrystalline analysis across a wide range of thermal conditions. At the lowest scale, a dislocation density-based crystal plasticity model is employed to capture the plastic response of the $\gamma\gamma'$ subgrain microstructure. Accounting for all the precipitates in every crystal of a multi-grain microstructure becomes computationally extensive after including only a small number of grains. Therefore, a parametric homogenisation scheme is utilised to manifest a single-crystal constitutive law that includes functional forms of the subgrain behaviour governing hardening and yield. An activation energy-based crystal plasticity framework is adopted for the homogenised grain-scale constitutive laws. This model is implemented at the polycrystalline scale to incorporate the effects of the $\gamma\gamma'$ while retaining the computational efficiency required to conduct studies at a length scale that would otherwise include thousands of individual precipitates.

Two-phase dislocation density-based model for the subgrain $\gamma\gamma'$ scale

A dislocation density-based crystal plasticity formulation is used to model $\gamma\gamma'$ microstructures of different sizes and morphologies. An overview is provided, but full details can be found in[5,24]. The plastic slip rate $\dot{\gamma}^\alpha$ on a given slip system α follows the Orowan equation $\dot{\gamma}^\alpha = \rho^\alpha_{\mathrm{M}} b v^\alpha$ where ρ^α_{M} is the mobile dislocation density, b is the Burgers vector and v^α is the dislocation velocity. Activation of plastic slip is permitted on both the octahedral and cube slip systems. The velocity of dislocations on slip system α is expressed as a thermally activated process and can be written as:

$$v^\alpha = v^\alpha_0 \exp\left(-\frac{Q}{k_{\mathrm{B}}T}\right)\sinh\left(\frac{\tau^\alpha_{\mathrm{eff}}}{\tau^\alpha_{\mathrm{cut}}}\right)\mathrm{sign}(\tau^\alpha) \qquad (1)$$

where v^α_0 is the initial velocity, Q is the activation energy, T is the temperature, $\tau^\alpha_{\mathrm{eff}}$ is the effective resolved shear stress defined as $\tau^\alpha_{\mathrm{eff}} = |\tau^\alpha| - \tau^\alpha_{\mathrm{pass}} - \tau^\alpha_{\mathrm{c}}$ when slip occurs, τ^α is the resolved shear stress, $\tau^\alpha_{\mathrm{pass}}$ is the passing stress, $\tau^\alpha_{\mathrm{cut}}$ is the cutting stress and τ^α_{c} is a critical shear stress discussed below. The slip resistances $\tau^\alpha_{\mathrm{pass}}$ and $\tau^\alpha_{\mathrm{cut}}$ provide the interaction stresses induced by in-plane (parallel) and out-of-plane

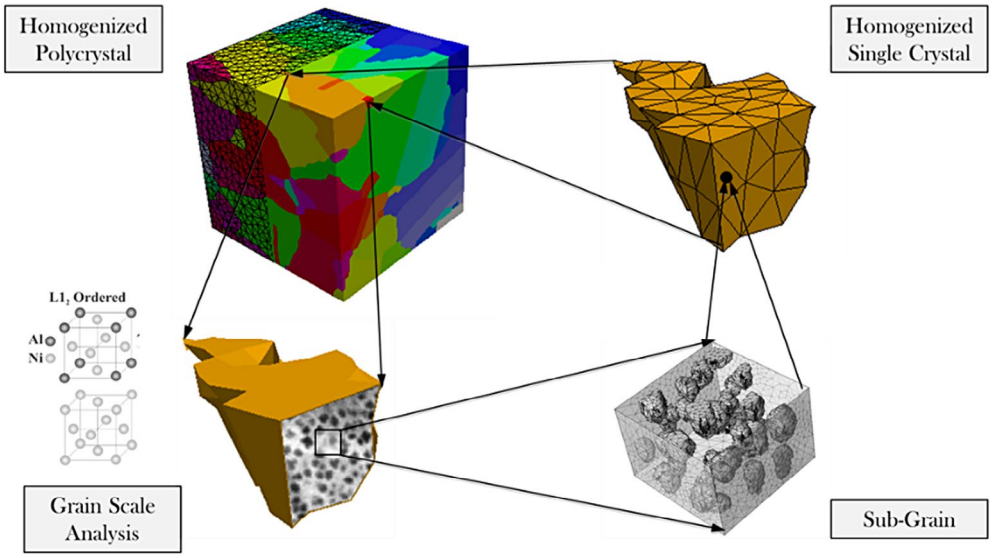

1 Schematic representation of multiple scales in the development of a crystal plasticity finite element model for Ni-based superalloys: polycrystalline microstructure, subgrain microstructure in a single grain, discretised subgrain microstructural RVE and homogenised crystal plasticity FE model for a grain

(forest) dislocations, respectively.[5,25] Each resistance stress is expressed in terms of these dislocation densities as:

$$\tau^{\alpha}_{pass} = c_2 \mu b \sqrt{\rho^{\alpha}_P + \rho^{\alpha}_M}, \tau^{\alpha}_{cut} = \frac{c_3 k_B T}{b^2} \sqrt{\rho^{\alpha}_F} \qquad (2)$$

where c_2 and c_3 are material constants, μ is the shear modulus and $\rho^{\alpha}_{\mathrm{P}}$ and $\rho^{\alpha}_{\mathrm{F}}$ are the parallel and forest dislocation densities, respectively. The evolution of these projected dislocation densities is formulated in terms of rate equations for statistically stored dislocations (SSDs) and geometrically necessary dislocations (GNDs), given in[6]. Therefore, the time evolution of SSDs and GNDs governs a portion of the overall hardening and yield behaviour of the material. The final consideration is a criterion for APB shearing which will account for non-Schmid effects on the octahedral slip systems. The APB shearing criterion is given as:

$$\tau^{\alpha}_{\mathrm{eff}} = \begin{cases} 0 & \text{for } |\tau^{\alpha}| - \tau^{\alpha}_{\mathrm{pass}} \le \tau^{\alpha}_{\mathrm{c}} \\ |\tau^{\alpha}| - \tau^{\alpha}_{\mathrm{pass}} - \tau^{\alpha}_{\mathrm{c}} & \text{for } |\tau^{\alpha}| - \tau^{\alpha}_{\mathrm{pass}} > \tau^{\alpha}_{\mathrm{c}} \end{cases} \qquad (3)$$

where $\tau^{\alpha}_{\mathrm{eff}}$ is the effective resolved shear stress and the critical shear stress is:

$$\tau^{\alpha}_{\mathrm{c}} = \begin{cases} \tau^{\alpha}_{\mathrm{c,oct}} = \tau^{\alpha}_{\mathrm{c,oct}}(\tau^{\alpha}_{\mathrm{pe}}, \tau^{\alpha}_{\mathrm{se}}, \tau^{\alpha}_{\mathrm{cb}}, T, \Gamma^{111}, \Gamma^{010}) & \text{on octahedral slip systems} \\ \tau^{\alpha}_{\mathrm{c,cube}} = \tau^{\alpha}_{\mathrm{c,cube}}(T) & \text{on cube slip systems} \end{cases} \qquad (4)$$

where $\tau^{\alpha}_{\mathrm{pe}}$ and $\tau^{\alpha}_{\mathrm{se}}$ are the shear stresses resolved onto the primary and secondary octahedral planes, $\tau^{\alpha}_{\mathrm{cb}}$ is the shear stress on the cross slip cube plane and Γ^{111} and Γ^{010} are the APB energies on the octahedral and cube planes. These non-Schmid shear stresses are necessary in forming a quantitative description of the KW lock configuration. The cross slip activation enthalpy is a function of $\tau^{\alpha}_{\mathrm{pe}}$, $\tau^{\alpha}_{\mathrm{se}}$ and $\tau^{\alpha}_{\mathrm{cb}}$, which are the resolved shear stresses that extend or constrict the locked superdislocation core, and the APB energies on the octahedral and cube planes.[15,26,27] This enthalpy provides a cross slip dislocation density rate which can be formulated as a total shear resistance due to cross slip locking events.[24,26] Since the probability of dislocation lock formation increases with increase in temperature, larger stresses are necessary at high temperatures to overcome the additional pinned obstacles. However, a competing mechanism causing obstacle strength reduction occurs simultaneously. As temperature increases and with sufficient applied stress, dislocation glide begins to occur along cube slip systems where the planes are not close packed. This secondary mechanism typically dominates after a critical temperature near 1000 K for superalloys and causes a drastic reduction in the yield strength.

The implementation of these constitutive laws has been executed in Ref. 22. Constant strain rate and creep simulations are calibrated to single-crystal experiments to provide the necessary material constants for the dislocation density evolution relations. A wide range of validation simulations are performed over various strain rates, temperatures, orientations and loading profiles.

Parametrically homogenised crystal plasticity model for single-crystal response

With the objective of thermo-mechanical analysis at the polycrystalline scale, the subgrain constitutive model is framed in a computationally tractable manner. Explicit precipitates in the two-phase microstructure are parametrically represented in a homogenised constitutive law with resistance parameters expressed as functions of the subgrain morphology.[5,22] The grain-scale model is an activation energy-based crystal plasticity framework developed in[1–3,5,6,28]. Plastic slip rate $\dot{\gamma}^{\alpha}$ in this model is governed by the Orowan's equation and adheres to a thermal activation relationship. For a given slip system,

$$\dot{\gamma}^{\alpha} = \begin{cases} 0 & \text{for } \tau^{\alpha}_{\mathrm{eff}} \le 0 \\ \dot{\gamma}^{\alpha}_{*} \exp\left(-\frac{Q}{k_{\mathrm{B}}T}\left[1 - \left(\frac{\tau^{\alpha}_{\mathrm{eff}}}{s^{\alpha}_{*,\mathrm{tot}}}\right)^{p}\right]^{q}\right)\mathrm{sign}(\tau^{\alpha}) & \text{for } 0 < \tau^{\alpha}_{\mathrm{eff}} \le s^{\alpha}_{*,\mathrm{tot}} \end{cases} \qquad (5)$$

where $\dot{\gamma}^{\alpha}_{*}$ is the reference slip rate and q and p are material constants. The effective shear stress is defined as $\tau^{\alpha}_{\mathrm{eff}} = |\tau^{\alpha}| - s^{\alpha}_{\mathrm{a}}$ where the athermal obstacles on the slip plane such as parallel dislocations result in an athermal slip resistance s^{α}_{a}. The total thermal slip resistance is comprised of two parts, viz.

$s^{\alpha}_{*,\mathrm{tot}} = s^{\alpha}_{*} + s^{\alpha}_{\mathrm{cross}}$. The thermal slip resistance s^{α}_{*} provides an impeding effect of obstacles that can be overcome by thermally activated processes such as forest dislocations, while the cross slip resistance $s^{\alpha}_{\mathrm{cross}}$ develops due to sessile dislocation segments creating pinning points by formation of KW configurations. The reference strain rate $\dot{\gamma}^{\alpha}_{*}$ is composed as a function of plastic strain to control the transition at the yield point[28] as:

$$\dot{\gamma}^{\alpha}_{*} = \dot{\gamma}_0 \left\{ \frac{\tanh(k) + \tanh(k l_{\mathrm{p}})}{10\{\tanh[k_{*}(\bar{\varepsilon}_{\mathrm{p}} - l_{\mathrm{p}})] + \tanh(k l_{\mathrm{p}})\}} - 1 \right\} H(\bar{\varepsilon}_{\mathrm{p}} - l_{\mathrm{p}}) + \dot{\gamma}_0 \tag{6}$$

where H is the Heaviside step function, $\dot{\gamma}_0$ is the initial plastic slip rate, l_{p}, k and k_{*} are material constants and $\bar{\varepsilon}_{\mathrm{p}}$ is the equivalent plastic strain defined as $\bar{\varepsilon}_{\mathrm{p}} = \sqrt{\frac{2}{3} E^{\mathrm{p}} : E^{\mathrm{p}}}$, where $E^{\mathrm{p}} = \frac{1}{2}(F^{\mathrm{pT}} F^{\mathrm{p}} - I)$ and F^{p} is the plastic deformation gradient.

The time evolution of the athermal and thermal slip resistances is given as a function of the plastic slip rate, in and out of the slip plane, corresponding to the effects of parallel and forest dislocations, respectively. The slip resistances evolve as:

$$\dot{s}^{\alpha}_{\mathrm{a}} = \sum_{\beta=1}^{N} h^{\alpha\beta}_{\mathrm{a}} |\dot{\gamma}^{\beta} \sin(\mathbf{n}^{\alpha}, \mathbf{t}^{\beta})| \tag{7}$$

and

$$\dot{s}^{\alpha}_{*} = \sum_{\beta=1}^{N} h^{\alpha\beta}_{*} |\dot{\gamma}^{\beta} \cos(\mathbf{n}^{\alpha}, \mathbf{t}^{\beta})| \tag{8}$$

where N is the number of slip systems, $\mathbf{m}^{\alpha}$ is the slip direction, $\mathbf{n}^{\alpha}$ is the slip plane normal, $\mathbf{t}^{\alpha} = \mathbf{m}^{\alpha} \times \mathbf{n}^{\alpha}$ and $h^{\alpha\beta}_{\mathrm{a}}$, $h^{\alpha\beta}_{*}$ are hardening coefficients that describe the interaction between dislocations along different slip systems, α and β. For simplicity, the interaction coefficients are equated for both the athermal and thermal cases, $h^{\alpha\beta} = h^{\alpha\beta}_{\mathrm{a}} = h^{\alpha\beta}_{*}$. The self and latent hardening are expressed as:

$$h^{\alpha\beta} = q^{\alpha\beta} h^{\beta}, \text{ where } h^{\beta} = h_0 \left| 1 - \frac{s^{\beta}}{s^{\beta}_{\mathrm{sat}}} \right|^{r} \mathrm{sign}\left(1 - \frac{s^{\beta}}{s^{\beta}_{\mathrm{sat}}} \right) \tag{9}$$

where h_0 is a material constant, $s^{\alpha} = \sqrt{(s^{\alpha}_{\mathrm{a}})^2 + (s^{\alpha}_{*})^2}$, $s^{\alpha}_{\mathrm{sat}}$ is the saturation slip resistance, r is an exponent controlling the rate of saturation and $q^{\alpha\beta} = q + (1 - q)\delta^{\alpha\beta}$ where $q = 1.4$. The hardening variables s^{α}_{*0}, k, k_{*}, $s^{\alpha}_{\mathrm{sat}}$ will be linked to the lower scale constitutive model by functional dependence on the morphological parameters of the $\gamma\gamma'$ microstructure.

The second contribution to the total thermal slip resistance is derived from the resistance $s^{\alpha}_{\mathrm{cross}}$ corresponding to the accumulation of pinned screw dislocations after cross slip.[6,24] The evolution of the cross slip resistance is an extension of the subgrain formulation and is computed for both the octahedral and cube slip systems as:

$$s^{\alpha}_{\mathrm{cross}} = \begin{cases} s^{\alpha}_{\mathrm{cross,oct}} = s^{\alpha}_{\mathrm{cross,oct}}(\tau^{\alpha}_{\mathrm{pe}}, \tau^{\alpha}_{\mathrm{se}}, \tau^{\alpha}_{\mathrm{cb}}, T, \Gamma^{111}, \Gamma^{010}) & \text{on octahedral slip systems} \\ s^{\alpha}_{\mathrm{cross,cube}} = s^{\alpha}_{\mathrm{cross,cube}}(T) & \text{on cube slip systems} \end{cases} \tag{10}$$

The cross slip resistance on the octahedral planes accounts for the non-Schmid shear stresses and anisotropy in the APB energy[24,26] and is expressed as:

$$s^{\alpha}_{\mathrm{cross,oct}} = \xi_0 \exp\left(\frac{A}{T - T_{\mathrm{c}}} \right) \mu \sqrt{\rho_{\mathrm{cross}}} \tag{11}$$

where

$$\rho_{\mathrm{cross}} = \rho_{\mathrm{cross},0} \exp\left(-\frac{H^{\alpha}}{k_{\mathrm{B}} T} \right) \tag{12}$$

and

$$H^{\alpha} = c_{\mathrm{H}} \left\{ h + k_1 (t^{\alpha}_{\mathrm{pe}} - k_2 t^{\alpha}_{\mathrm{se}}) + \sqrt{\left(\frac{1}{\sqrt{3}} - \frac{\Gamma^{010}}{\Gamma^{111}} + |t^{\alpha}_{\mathrm{cb}}| \right) \frac{b}{B}} \right\} \tag{13}$$

where ξ_0, A, h, k_1 and k_2 are material constants, T_{c} is the critical temperature, H^{α} is the enthalpy for the cross slip event, ρ_{cross} is the cross slip dislocation density, $\rho_{\mathrm{cross},0}$ is the initial cross slip dislocation density and

$$t^{\alpha}_{\mathrm{xx}} = \frac{\tau^{\alpha}_{\mathrm{xx}}}{\Gamma^{111}/b}, B = \frac{\mu b^2}{2\pi\Gamma^{111}}, c_{\mathrm{H}} = \frac{\mu b^3}{4\pi}.$$

This cross slip resistance envelops a competition between additional hardening due to further generation of cross slipped sessile dislocations and a weakening due to a reduction in obstacle strength as temperature increases. At the peak temperature, the latter mechanism overcomes the strengthening from locked dislocations. The necessary input parameters have been experimentally calibrated in[24] and given in Tables 1 and 2. The remainder of the terms are controlled by the homogenised morphological hardening variables given below.

A computational procedure for parametric homogenisation is implemented to create a functional dependence between the terms of the constitutive law and subgrain morphological parameters.[5,22] The subgrain microstructure, comprised of γ' precipitates in a γ matrix, is constructed as a

Table 1 Input material constants for grain-scale constitutive model

Parameter	h	Γ^{010} (J/m^{-2})	Γ^{111} (J/m^{-2})	b (m)	μ (GPa)	$\rho_{\mathrm{cross},0}$ (m^{-2})
Value	0.3	0.083	0.3	2.49×10^{-10}	142.2	5.0×10^{15}

Table 2 Calibrated material constants for grain-scale constitutive model

Parameter	k_1	k_2	ξ_0	A	T_{c}	Q (J)	p	q	$\dot{\gamma}_0$ (s^{-1})	h_0 (MPa)	r
Value	0.4	0.6	8	325	1600	6.5×10^{-19}	0.78	1.15	5×10^{7}	100	1.115

RVE. The morphology of the configuration is characterised by the volume fraction of the γ' phase, the channel width l_c between γ' precipitates and a γ' shape exponent. The shape exponent n is the exponent of the superellipsoid equation $\left(\frac{x}{a}\right)^n + \left(\frac{y}{b}\right)^n + \left(\frac{z}{c}\right)^n = 1$where a, b and c are the half lengths of the principal axes and assumed to be equal, i.e. $a = b = c$. Varying the value of n from 2 to ∞ corresponds to changing the precipitates' shapes from spheres to cubes. In order to avoid the singularity for the cubic case, a transformed shape factor $n_1 = \tan^{-1}(n)$ is chosen.

Through a sensitivity analysis of the subgrain $\gamma\gamma'$ simulations, variations in the γ' volume fraction v_p, channel width l_c and shape factor n_1 cause different hardening and yield behaviour due to changes in the evolving dislocation densities. These responses are captured by the grain-scale constitutive law through the parameters s^α_a, s^α_* and s^α_{cross}. Therefore, a link can be made between these parameters and the changes to the subgrain morphology. The objective of parametric homogenisation is to determine the relationships for the initial thermal slip resistance s^α_{*0}, the material constants k and k_* that control the reference slip rate $\dot{\gamma}^\alpha_*$, the saturation stress s^α_{sat} and a factor $s^\alpha_{cross,0}$ that is multiplied with the computed s^α_{cross} as functions of v_p, l_c and n_1. Computational homogenisation is performed by executing a large set of simulations with various volume fractions, channel widths and shapes.[5,22] Functional forms of the hardening parameters are determined by satisfying micro–macro homogeneity conditions[29] in[6]. The homogenised set of parameters, $s^\alpha_{*0}(v_p, l_c, n_1)$, $k(v_p, l_c, n_1)$, $k_*(v_p, l_c, n_1)$, $s^\alpha_{sat}(v_p, l_c, n_1)$ and $s^\alpha_{cross,0}(v_p, l_c, n_1)$, are derived to have the following forms:

$$\begin{aligned} s^\alpha_{*0}(n_1, v_p, l_c) &= a_1(n_1, v_p) + \frac{b_1(n_1, v_p)}{\sqrt{l_c}} \\ &= -50.32 v_p n_1 + 221.63 v_p - 33.63 n_1 + 384.43 \\ &\quad + \frac{-33.3 v_p n_1 + 32.92 v_p + 19.61 n_1 - 0.037}{\sqrt{l_c}} \\ s^\alpha_{sat}(n_1, v_p, l_c) &= a_2(n_1, v_p) + \frac{b_2(n_1, v_p)}{l_c} \\ &= 6680 v_p n_1 - 8905 v_p - 1648 n_1 + 3185 \\ &\quad + \frac{-3599 v_p n_1 + 5008 v_p + 363 n_1 - 0.21}{l_c} \end{aligned}$$

$$\begin{aligned} k_*(n_1, v_p, l_c) &= 19847 v_p n_1 l_c + 12768 v_p n_1 - 23120 v_p l_c \\ &\quad + 4080 n_1 l_c - 7500 v_p + 33 n_1 - 2700 l_c + 65 \\ k(n_1, v_p, l_c) &= a_3(n_1, v_p) + \frac{b_3(n_1, v_p)}{\sqrt{l_c}} \\ &= 221.4 v_p n_1 - 327.6 v_p + 31.5 n_1 + 5.5 \\ &\quad + \frac{-176.5 v_p n_1 + 281.2 v_p - 2.44 n_1 + 0.14}{\sqrt{l_c}} \end{aligned}$$

$$\begin{aligned} s^\alpha_{cross}(n_1, v_p, l_c) &= s^\alpha_{cross} \times s_0(n_1, v_p, l_c), s_{cross,0}(n_1, v_p, l_c) \\ &= a_1(n_1, v_p) + \frac{b_1(n_1, v_p)}{\sqrt{l_c}} \\ &= -0.130895 v_p n_1 + 0.538 v_p - 0.09528 n_1 + 1 \\ &\quad + \frac{-0.08662 v_p n_1 + 0.08566 v_p + 0.051 n_1 - 0.000096}{\sqrt{l_c}} \end{aligned} \quad (14)$$

This complete procedure provides a validated grain-level constitutive law with an implicit representation of the subgrain morphology through functional dependencies of the slip and hardening parameters.

Analysis of polycrystalline microstructures with parametrically homogenised crystal plasticity model

The parametrically homogenised activation energy-based crystal plasticity constitutive model for Ni-based superalloys is applied to individual grains of a polycrystalline microstructure. A parametric study of ambient thermal conditions is performed to connect the thermo-mechanical micro-mechanisms to the response of the polycrystalline model. The objective is to demonstrate that the slip mode transition due to dislocation core effects has a tremendous influence on the crucial mechanical quantities at this higher scale.

Polycrystalline Rene88-DT, an industrial-grade Ni-based superalloy, is used as a model superalloy for analysis in this paper. The volume fraction of γ' is about 42%, with a channel width of about 0.200 μm, and spheroidal particles corresponding to a shape exponent $n = 5$.[30,31] These values parametrise the subgrain morphology corresponding to the example geometry in Fig. 2 and influence the hardening and yield variables of the single-crystal constitutive law. Substituting these subgrain descriptors into the homogenised functional forms from equation (14), the parameters of the activation energy-based model are determined to be

$$s^\alpha_{*,0} = 450.41\,\text{MPa}, k = 68.134, k_* = 5253.5,$$
$$s^\alpha_{sat} = 4355.4\,\text{MPa}, \text{ and } s^\alpha_{cross,0} = 1.1447$$

Throughout this study, the transition of slip mode from octahedral to cube determines important mechanical behaviour. In general, there is some disagreement over the exact role of cube slip in the two-phase system, and the primary mechanisms by which it propagates in the γ phase, γ' phase and interfaces between the precipitates and matrix. However, sufficient experimental evidence is reported to support the activation of cube slip in both phases to some degree[32–38] for single crystals and polycrystals of Ni-based superalloys.

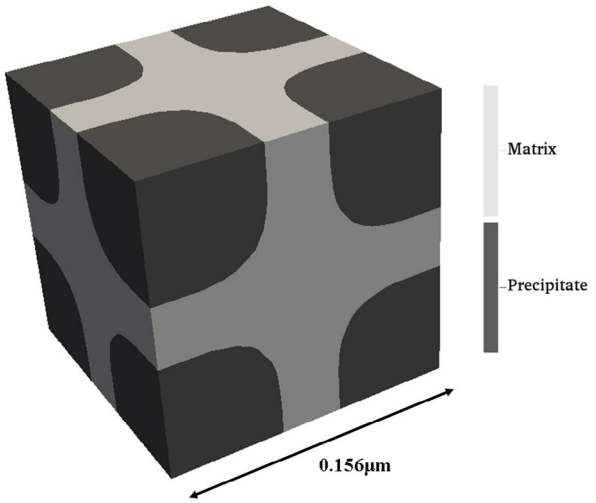

2 An example $\gamma\gamma'$ subgrain microstructure of Rene88-DT with v_f = 42%, l_c = 200 nm and n = 5 that controls the homogenised constitutive law for the polycrystalline simulations

Provided that dislocation slip occurs along cube slip systems in accordance with the multi-scale model framework and is more dominant than the unlocking of KW configurations onto octahedral planes, the implications of such a mechanism are analysed in the context of polycrystalline microstructures.

Aspects of octahedral and cube slip systems

For the following analysis, it is necessary to illustrate several fundamental concepts regarding octahedral and cube slip systems as a reference. Most importantly, maximum Schmid factor plots in Fig. 3*a* and *b* on standard triangles yield approximate indicators of orientations that experience the highest resolved shear stress, highlighting grains that would be likely candidates for plastic deformation. This first-order indicator fails as the stress tensor deviates from uniaxial stress and assumes the validity of Schmid's law for the material. Both of these criteria are challenged for polycrystalline Ni-based superalloys, but the plots will be shown to provide a reasonable intuition for the results. In addition, it is worth noting that all the standard triangles presented throughout this work are Lambert azimuthal equal area (LAEA) projections. The LAEA standard triangle differs from stereographic triangles in that it is an area preserving map from the surface of the sphere to the projection plane rather than an angle preserving map. This choice of projection has the visual benefit of mapping probability densities without distortion so that statistical inquiries can be observed readily by comparing areal densities. In a randomly oriented polycrystal, individual grains are more likely to have a maximum Schmid factor on an octahedral slip system (70% probability) rather than on a cube slip system as shown in Fig. 3*c*. The grains of the virtual microstructure are visualised on the standard triangle and designated by the loading axis in each grain's local crystal basis in Fig. 3*d*. Approximately 55% of these grains lie in the region corresponding to orientations favouring octahedral slip.

Virtual microstructure generation

A direct implementation method is performed to generate a 3D virtual microstructure of polycrystalline Ni-based superalloys to be prepared for finite element simulation. The overall procedure consists of acquiring and processing experimental microstructural data, filtering and smoothing geometrically problematic regions and meshing the resultant structure. A sample of Rene88-DT is provided by the group of Pollock et al.[31] in the form of electron back-scattered diffraction (EBSD) scans of serial sections, and the individual slices are reconstructed into a 3D microstructure. The crystallographic orientation of each grain in the virtual microstructure

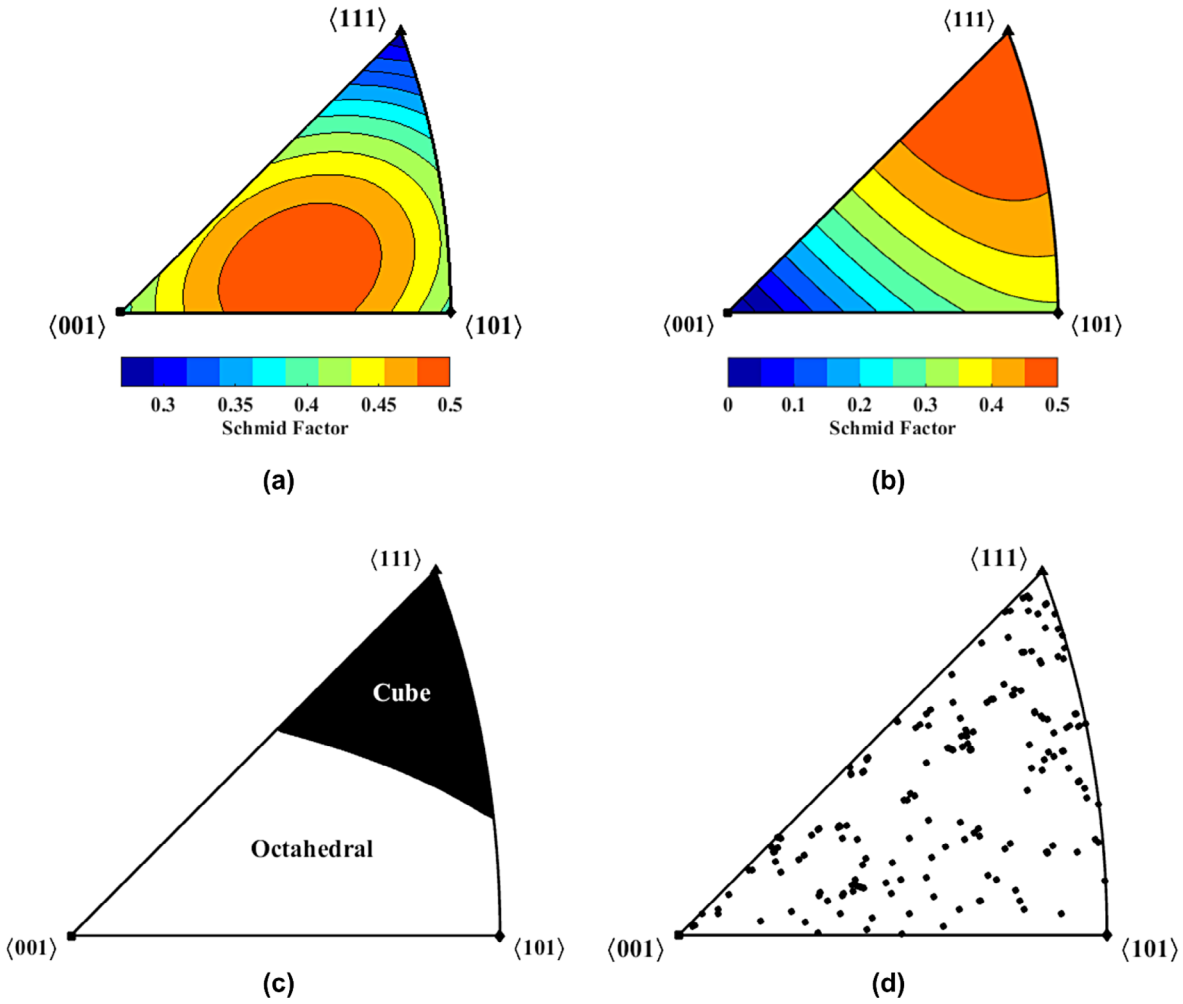

3 LAEA standard triangles depicting *a* maximum Schmid factors on octahedral slip systems, *b* maximum Schmid factors on cube slip systems, *c* orientations dominated by either octahedral or cube sip systems and *d* crystal loading orientation density plotting each grain of the virtual microstructure

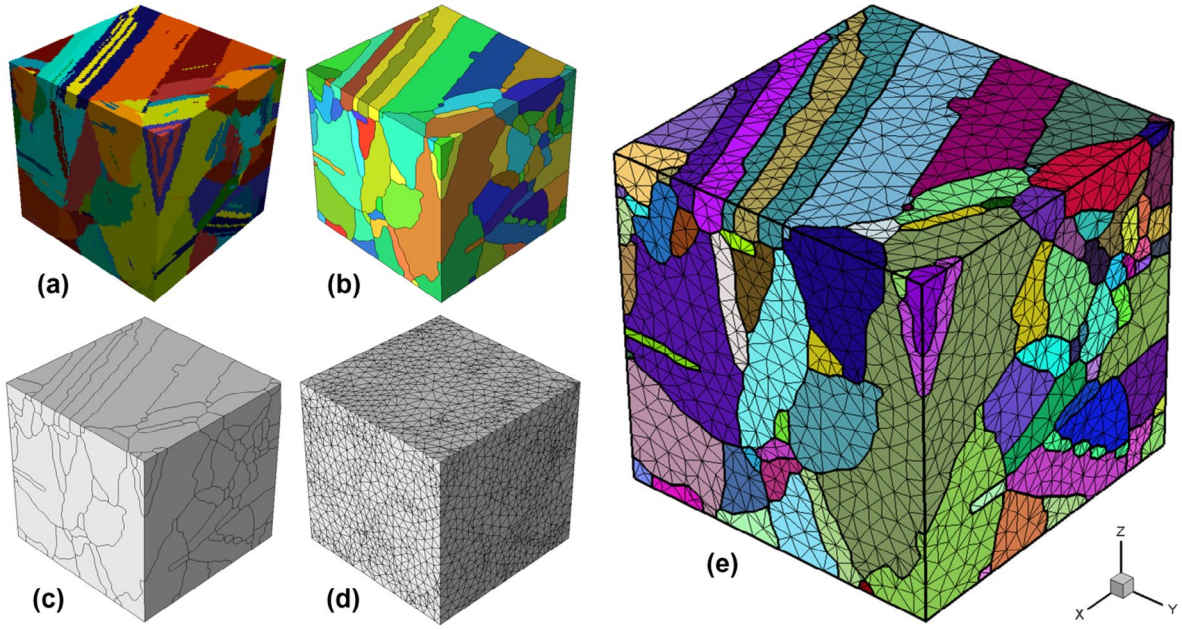

4 Reconstruction of virtual polcrystalline microstructure of Rene88-DT: *a* serial sectioned EBSD data, *b* application of filters such as minimum volume thresholding, erosion and dilation and edge and vertex processing, *c* boundary smoothing iterations, *d* refined meshing in localised regions and *e* final meshed polycrystalline microstructure including Σ3 annealing twins (each colour in the contour plot represents a unique grain ID)

is selected from the corresponding grain orientation in the EBSD data. The reconstructed microstructure is permeated with thin, high aspect ratio, annealing Σ3 twins that cause a multitude of issues for meshing and data processing approaches. The full procedure of acquiring a finite element mesh from EBSD data[39] uses microstructural and mesh generation software tools, DREAM.3D and Simmetrix.[40,41] The data processing methodology, illustrated in Fig. 4, is followed to prepare the experimental geometry for tetrahedral discretisation. The steps include minimum volume filters, erosion and dilation, edge refinement, vertex repositioning and refined meshing at critical locations. The final element mesh retains many of the high aspect ratio annealing twins and important local features inherent to a Rene88-DT sample, while also maintaining an optimised number of elements to provide both computational efficiency and accuracy.

Finite element simulations of the polycrystalline microstructures

The resultant finite element mesh consists of 206 grains, including twins, discretised into 99 975 degrees of freedom and 180 203 linear tetrahedral elements with an **F**-bar patch method enhancement to remove volumetric locking.[42] Uniaxial constant strain rate simulations are executed for various isotherms across a range of operating temperatures (300, 673, 923, 1073, 1173 and 1273 K). The microstructure is loaded in both tension and compression along the same axis at a strain rate of $10^{-4}s^{-1}$ for each temperature.

Numerical results

The polycrystalline simulations are performed to understand the transition in mechanical response and micro-mechanisms from room temperature to 1300 K. There is a change in slip mode from the octahedral to cube slip systems as temperature is increased, and this transition promotes a variety of

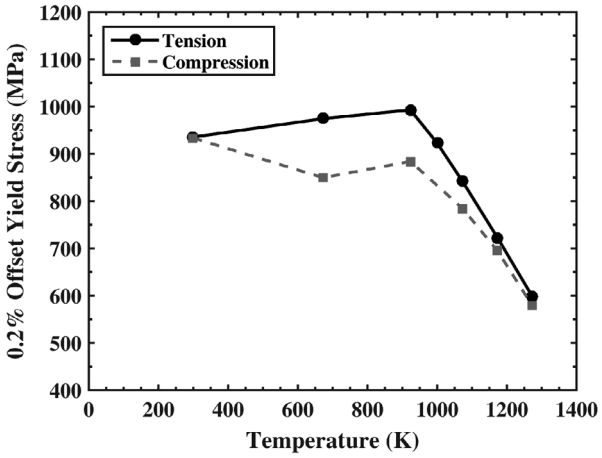

5 The 0.2% offset yield strength for both tension and compression constant strain rate tests on a polycrystalline superalloy microstructure illustrating the steady progression in strength at low and intermediate temperatures leading to a sudden drop after a peak temperature near 900–1000 K

microscale mechanisms. A dramatic shift occurs in the local yield strength, plastic strain and load-bearing capacity for oriented grains. Each of these mechanical effects has an important role in the aggregate material behaviour.

For both tension and compression tests, the 0.2% offset yield stress is determined for ambient temperatures of 300, 673, 923, 1073, 1173 and 1273 K as shown in Fig. 5. In tension, the general trend is a slight increase in strength until a critical peak temperature near 900–1000 K, where the strength begins to decrease severely. A similar response occurs for compression as well. However, an asymmetry is observed over the intermediate temperatures, which follows the behaviour of superalloy single crystals and $L1_2$ intermetallics.[13,26] Tension and compression cases agree at room temperature and high temperatures. These correspond to cases

where single-crystal experiments show no asymmetry since KW locks have minimal influence. Between these extremes, ⟨0 0 1⟩-oriented grains exhibit higher strengths in tension, ⟨1 0 1⟩ orientations favour compression and ⟨1 1 1⟩ show no bias. These phenomena are a direct consequence of the non-Schmid effects caused by KW configurations in the γ' phase and agree with the expected response of single-crystal experiments. For superalloys and $L1_2$ intermetallics, there is also a greater disparity in yield asymmetry for ⟨0 0 1⟩ grains. In this simulation, a higher volume fraction nearer to this orientation than ⟨1 0 1⟩ is observed leading to an overall larger strength for tension in the polycrystalline ensemble in Fig. 5. The final drop in yield strength at high temperatures is attributed to the release of KW locks by plastic flow along the cube planes.

The transition in slip mode with increasing temperature is indicated by the activation of plastic deformation on individual slip systems. For each grain, the accumulated plastic slip is volumetrically averaged on every slip system. The amount of slip on individual slip systems is compared to determine which slip system underwent maximum plastic flow. If this maximum value falls upon an octahedral slip system, the grain is designated an 'octahedral grain' and analogously for the case of cube slip systems, a 'cube grain'. The classification permits the study of the volume fraction of octahedral- and cube glide-dominated grains over a range of temperatures shown in Fig. 6. At low temperatures, the polycrystalline response is controlled by octahedral slip throughout the entire microstructure. As the peak temperature is approached, a shift in the slip mode begins to develop and a fraction of the grains becomes susceptible to plastic slip along the cube planes. With further increase in temperature, dislocation glide on the cube slip systems dominates the plastic response of the entire aggregate. There exists a strong correlation between the polycrystalline yield strength and the fraction of cube grains in the ensemble. For cube glide, no mechanism such as KW locks exists to prevent plasticity. Slip along these planes is promoted by elevated temperatures since dislocation motion is a thermally activated process. This facilitation of further

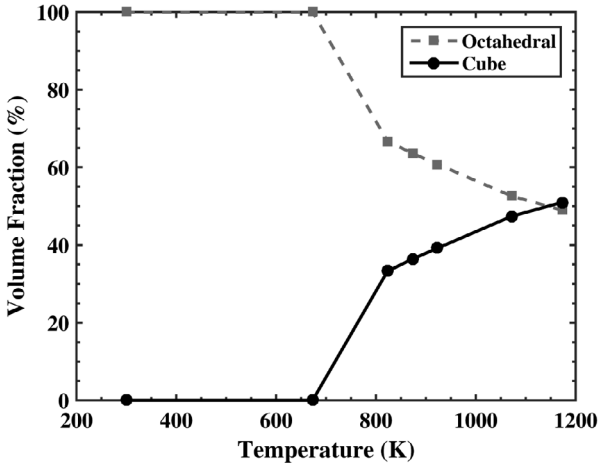

6 Volume fraction of polycrystalline microstructure with largest accumulated plastic slip on cube or octahedral slip systems computed at 3% total strain. As temperature increases, a significant slip mode transition occurs to favour plasticity along cube slip systems

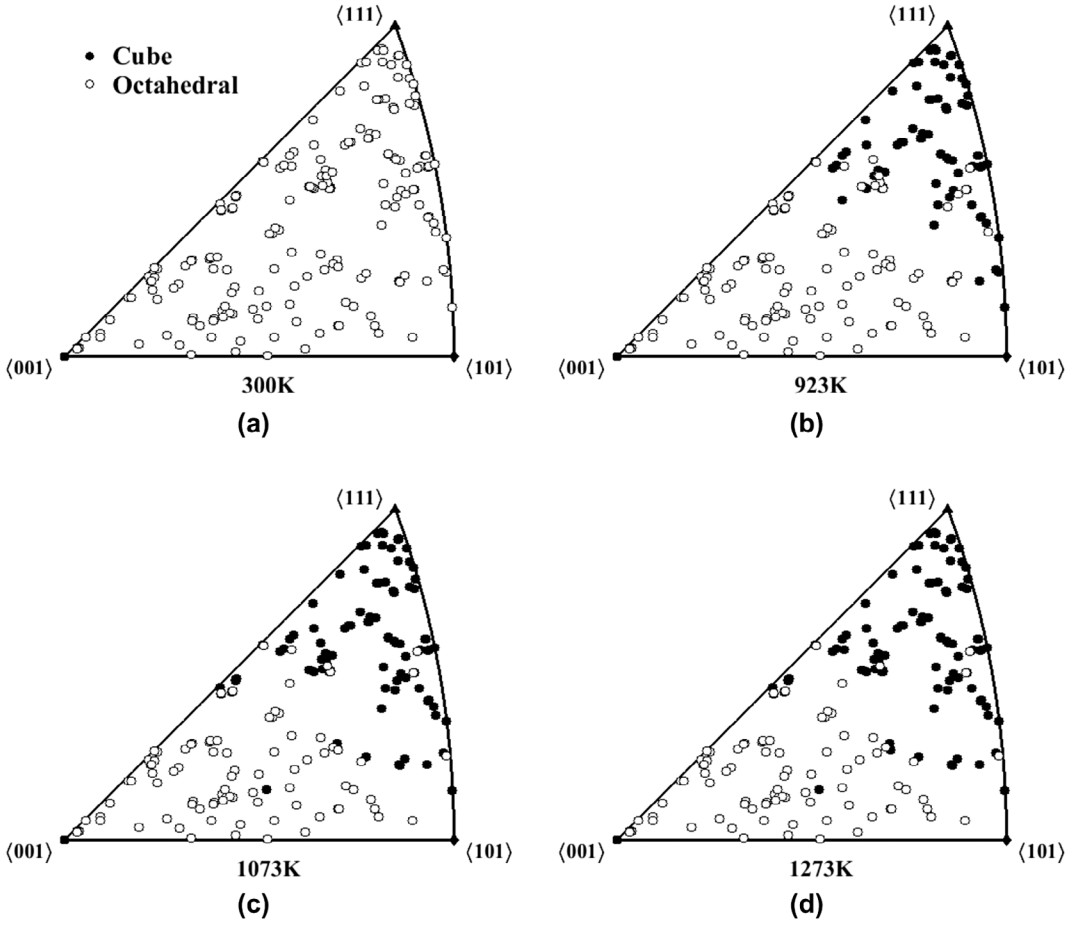

7 LAEA standard triangles demonstrating the progressive dominance of plastic slip on cube slip systems in grains with favourable loading orientation, i.e. near ⟨1 1 1⟩, as temperature increases from 300 to 1273 K

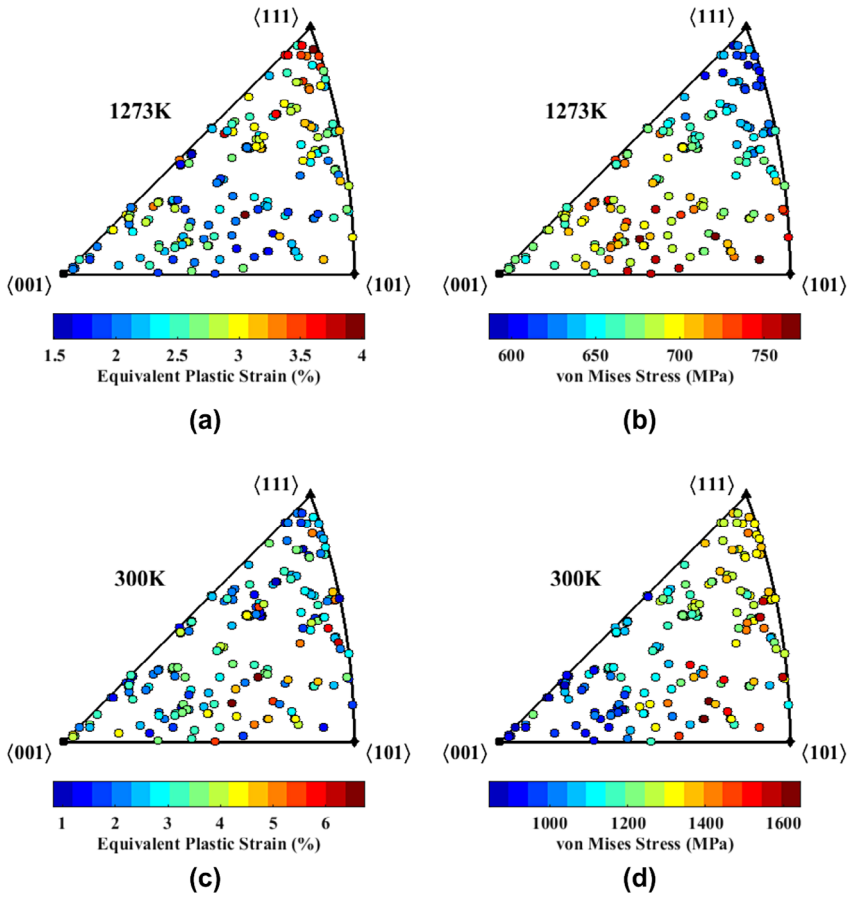

8 LAEA standard triangles showing, for each grain, the equivalent plastic strain and von Mises stress *a*, *b* at 1273 K and *c* and *d* at 300 K. The total strain is 3% in tension and a transition from load-bearing grains to plastically yielding grains is observed to be highly orientation and temperature dependent

plasticity demonstrates the connection between the weakening of the material and the activation of cube slip systems.

The polycrystalline simulations reveal an important role played by grains with cube dominated slip behaviour. It is essential to understand the conditions that favour this mechanism in order to help design a microstructure that could limit or intensify the process. Similar to the case for single crystals, the activation of dislocation glide along cube slip planes is highly dependent on crystal orientation. Due to the relatively large Schmid factor for cube planes and low Schmid factor for octahedral planes near ⟨1 1 1⟩ loading orientations in Fig. 3, the primary expectation is that grains with this orientation will be most vulnerable to cube slip. The polycrystalline simulations indicate that plasticity in ⟨1 1 1⟩ grains is, in fact, greatly influenced by slip along the cube planes. The standard triangles shown in Fig. 7 for various temperatures establish the growing dominance of cube slip as the material is deformed in the high temperature regime. The ⟨1 1 1⟩ grains are the first to transition slip modes as temperature increases. More octahedral grains convert to cube grains initiating from the ⟨1 1 1⟩ corner of the standard triangle and propagating to both the ⟨1 0 1⟩ and ⟨0 0 1⟩ corners in accordance with the contours of the maximum cube slip system Schmid factor in Fig. 3*b*. This trend reveals that the high-temperature yield response becomes largely governed by the presence of ⟨1 1 1⟩ grains in the ensemble.

A number of important inferences are made from the effect of grain orientation and its relation to slip mode transitions. Many mechanical events undergo a complete reversal in stress–strain behaviour as can be exemplified by an analysis of hard and soft grains in the polycrystalline microstructure. At low and intermediate temperatures, soft grains that experience substantial plastic deformation congregate in the general area of orientation space corresponding to maximum Schmid factor for octahedral slip systems. The majority of the equivalent plastic strain is sustained by individual grains spread over the range of orientations between ⟨0 0 1⟩ and ⟨1 0 1⟩ and away from ⟨1 1 1⟩ directions as seen in Fig. 8*c*. Since the behaviour at this temperature range is governed by octahedral slip systems and the activation of cube slip systems requires overcoming a large energy barrier, it is reasonable that the majority of plasticity concentrates in grains oriented with the highest resolved shear stress on octahedral slip systems, i.e. the region of the standard triangle between ⟨0 0 1⟩ and ⟨1 0 1⟩. It is noteworthy that there is not a clear concentration of plastic strain at the orientations with maximum octahedral Schmid factor, but instead, a smearing between ⟨0 0 1⟩ and ⟨1 0 1⟩ due to the non-Schmid effects at the single-crystal scale. At these lower temperatures, hard grains, load-bearing grains that remain resistant to plasticity, are identified by their stress state. The volumetrically averaged von Mises stress is shown for each grain in Fig. 8*d*. Since the ⟨0 0 1⟩ and ⟨1 0 1⟩ grains bear the majority of plastic flow, only the ⟨1 1 1⟩ grains remain to support the applied boundary conditions. Thus, the crystals with orientations near ⟨1 1 1⟩ act as hard grains in this temperature range and exhibit relatively large stress states. This outcome is understood through an interpretation of the von Mises stress, but is also ascertained for

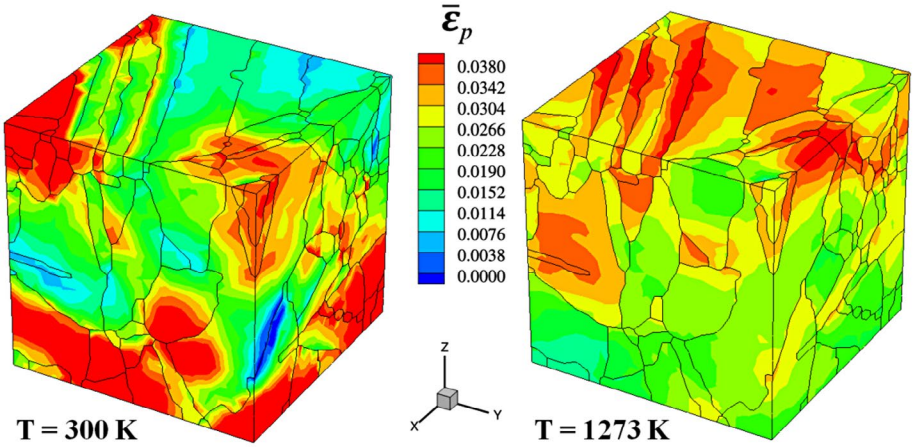

9 Contours of equivalent plastic strain on the same polycrystalline microstructure deformed to 3% total strain in tension at temperatures of 300 and 1273 K. A drastic shift is observed in the identification of grains undergoing the majority of plastic deformation

other stress measures such as the maximum principal stress and the normal stress component in the loading direction. As the temperature increases, the mechanical response of individual grains undergoes a complete reversal. The ⟨1 1 1⟩ grains, which were originally designated hard grains at low temperatures and carried the burden of the overall microstructural load, quickly lose their stress-enduring capacity and plastically yield as seen in Fig. 8*a* and *b*. On the other hand, the soft grains residing at the ⟨0 0 1⟩–⟨1 0 1⟩ regions of the standard triangle no longer sustain large plastic strains. Instead, they resist deformation and develop considerable amounts of stress.

The entire process described above is attributed to the transition of slip mode from octahedral to cube. An elevation in temperature is demonstrated to cause soft grains to become hard, and vice versa, inducing a drastic change, both mechanically and geometrically, to how the microstructure deforms and supports load. The severity of the transition in mechanical response is clearly depicted in Fig. 9. Almost every grain in the polycrystalline microstructure experiences a complete shift in its relative contribution to sustaining the total plastic flow.

Conclusions

A multi-scale constitutive framework for Ni-based superalloys is implemented to study the thermo-mechanical behaviour of polycrystalline microstructures through a parametric analysis of temperature response. The resulting parametrically homogenised activation energy-based crystal plasticity constitutive model is employed to capture the effects of important single-crystal phenomena such as non-Schmid effects, APB shearing and the influence of subgrain $\gamma\gamma'$ morphology. Parametric homogenisation of the constitutive model enables polycrystalline simulations while maintaining the detailed mechanical response of the $\gamma\gamma'$ substructures. An image-based polycrystalline microstructural model is loaded over a wide temperature range of 300–1300 K to understand the important consequences of slip mode transition on material performance. Due to dislocation mechanisms, the occurrence of plastic slip shifts from octahedral planes to cube planes at elevated temperatures. This transition is intimately linked to critical polycrystalline responses such as texture, overall yield strength, tension–compression asymmetry and selection of load-bearing grains. With increased temperature, cube slip becomes progressively more dominant in favourably oriented grains and causes a significant weakening of the entire microstructure. In addition, due to the connection between dislocation motion along cube planes and grains with ⟨1 1 1⟩ loading orientations, the designation of hard and soft grains undergoes a complete reversal. ⟨1 0 0⟩ and ⟨1 0 1⟩ grains are the anticipated sites for plastic deformation at low temperatures, but become highly stressed crystals as the temperature is increased. Simultaneously with temperature elevation, plastic strain is promoted on ⟨1 1 1⟩ grains. All these micromechanical effects demonstrate the importance of linking small-scale material behaviour to the microstructure design process. This polycrystalline model highlights specific links between microstructural features to the resultant mechanical response that can be valuable in achieving desired thermo-mechanical performance.

Acknowledgements

This work has been supported through a grant number FA9550-12-1-0445 to the Center of Excellence on Integrated Materials Modeling (CEIMM) at Johns Hopkins University awarded by the AFOSR/RSL Computational Mathematics Program (Manager Dr A. Sayir) and AFRL/RX (Monitors Dr C. Woodward and C. Przybyla). This sponsorship is gratefully acknowledged. Computational support of this work has been provided by the Homewood High Performance Compute Cluster (HHPC) at Johns Hopkins University.

Funding

This work has been supported by the Center of Excellence on Integrated Materials Modeling (CEIMM) at Johns Hopkins University [grant number FA9550-12-1-0445].

References

1. U. F. Kocks, A. S. Argon and M. F. Ashby: 'Thermodynamics and kinetics of slip', *Prog. Mater. Sci.*, 1975, **19**, 110–170.
2. E. P. Busso: 'Cyclic deformation of monocrystalline nickel aluminide and high temperature coatings', PhD thesis, Massachusetts Institute of Technology, Cambridge, MA, USA, 1990.
3. E. P. Busso and F. A. McClintock: 'Gradient-dependent viscoplastic deformation of two-phase single crystals', *Int. J. Plast.*, 1996, **12**, 1–28.

4. E. P. Busso, F. Meissonnier and N. P. O'Dowd: 'A dislocation mechanics-based crystallographic model of a b2-type intermetallic alloy', *J. Mech. Phys. Solids*, 2000, **48**, (11), 2333–2361.
5. S. Keshavarz and S. Ghosh: 'Multi-scale crystal plasticity finite element model approach to modeling nickel-based superalloys', *Acta Mater.*, 2013, **61**, (17), 6549–6561.
6. S. Keshavarz, S. Ghosh, A. Reid and S. Langer: 'A non-Schmid crystal plasticity finite element approach to multi-scale modeling of nickel-based superalloys', *Acta Mater.*, 2016, **114**, (1), 106–115.
7. R. Lowrie: 'Mechanical properties of intermetallic compounds at elevated temperatures', *Trans. Am. Inst. Min. Metall. Eng.*, 1952, **194**, 1093–1100.
8. J. H. Westbrook: 'Temperature dependence of the hardness of secondary phases common in turbine bucket alloys', *J. Met.*, 1957, **209**, 898–904.
9. P. A. Flinn: 'Theory of deformation in superlattices', *Trans. Am. Inst. Min. Metall. Eng.*, 1960, **218**, (1), 145–154.
10. P. H. Thornton, R. G. Davies and T. L. Johnston: 'The temperature dependence of the flow stress of the γ phase based upon Ni_3Al', *Metall. Trans.*, 1970, **1**, (1), 207–218.
11. S. S. Ezz, D. P. Pope and V. Paidar: 'The tension/compression flow stress asymmetry in Ni_3(Al,Nb) single crystals', *Acta Metall.*, 1982, **30**, (5), 921–926.
12. F. E. Heredia and D. P. Pope: 'Solid solution strengthening of Ni_3Al by B and Hf additions', *J. Phys. III*, 1991, **1**, (6), 1055–1064.
13. F. E. Heredia: 'Solid solution strengthening and fracture of Ni_3Al single crystals', PhD thesis, University of Pennsylvania, Philadelphia, PA, USA, 1990.
14. F. E. Heredia and D. P. Pope: 'The plastic flow of binary Ni_3Al single crystals', *Acta Metall. Mater.*, 1991, **39**, (8), 2027–2036.
15. V. Paidar, D. P. Pope and V. Vitek: 'A theory of the anomalous yield behavior in $L1_2$ ordered alloys', *Acta Metall.*, 1984, **32**, (3), 435–448.
16. S. V. Takeuchi and E. Kuramoto: 'Temperature and orientation dependence of the yield stress in Ni_3Ga single crystals', *Acta Metall.*, 1973, **21**, (4), 415–425.
17. P. Veyssiare and G. Saada: 'Microscopy and plasticity of the $L1_2$ γ' phase', *Dislocat. Solids*, 1996, **10**, 253–441.
18. D. M. Dimiduk: 'Dislocation structures and anomalous flow in $L1_2$ compounds', *J. Phys. III*, 1991, **1**, (6), 1025–1053.
19. R. Reed: 'The superalloys', Cambridge University Press, Birmingham, UK, 2006.
20. D. P. Pope and S. S. Ezz: 'Mechanical properties of Ni_3Al and nickel-base alloys with high volume fraction of γ'', *Int. Met. Rev.*, 1984, **29**, (1), 136–167.
21. B. H. Kear: 'Dislocation configurations and work hardening in Cu_3Au crystals', *Acta Metall.*, 1964, **12**, (5), 555–569.
22. S. Keshavarz and S. Ghosh: 'Hierarchical crystal plasticity FE model for nickel-based superalloys: sub-grain microstructures to polycrystalline aggregates', *Int. J. Solids Struct.*, 2015, **55**, 17–31.
23. S. Ghosh and S. Keshavarz: 'Multi-scale crystal plasticity FEM approach to modeling nickel-based superalloys', Proc. 55th AIAA/ASMe/ASCE/AHS/SC Structures, Structural Dynamics, and Materials Conference, Baltimore, MD, USA, 2014, AIAA.
24. S. Keshavarz and S. Ghosh: 'A crystal plasticity finite element model for flow stress anomalies in Ni_3Al single crystals', *Philos. Mag.*, 2015, **95**, (24), 2639–2660.
25. A. Ma and F. Roters: 'A constitutive model for FCC single crystals based on dislocation densities and its application to uniaxial compression of aluminium single crystals', *Acta Mater.*, 2004, **52**, (12), 3603–3612.
26. C. Allan: 'Plasticity of nickel base single crystal superalloys', PhD thesis, Massachusetts Institute of Technology, Cambridge, MA, USA, 1995.
27. A. M. Cuitiño and M. Ortiz: 'Constitutive modeling of $L1_2$ intermetallic crystals', *Mater. Sci. Eng.: A*, 1993, **170**, (1–2), 111–123.
28. C. L. Xie, S. Ghosh and M. Groeber: 'Modeling cyclic deformation of HSLA steels using crystal plasticity', *J. Eng. Mater. Technol.*, 2004, **126**, (4), 339–352.
29. R. Hill: 'On macroscopic effects of heterogeneity in elastoplastic media at finite strain', Mathematical Proceedings of the Cambridge Philosophical Society, Cambridge, UK, 1984, Cambridge University Press, Vol. 95, 481–494.
30. J. MacSleyne, M. D. Uchic, J. P. Simmons and M. De Graef: 'Three-dimensional analysis of secondary $\gamma'\gamma'$ precipitates in René-88 DT and UMF-20 superalloys', *Acta Mater.*, 2009, **57**, (20), 6251–6267.
31. W. Lenthe, M. Echlin and T. Pollock. Unpublished data, 2015.
32. M. R. Daymond, M. Preuss and B. Clausen: 'Evidence of variation in slip mode in a polycrystalline nickel-base superalloy with change in temperature from neutron diffraction strain measurements', *Acta Mater.*, 2007, **55**, (9), 3089–3102.
33. N. Clément, A. Couret and D. Caillard: 'An in situ study of cube glide in the γ'-phase of a superalloy', *Philos. Mag. A*, 1991, **64**, (3), 669–695.
34. D. Bettge and W. Osterle: '"Cube slip" in near-[111] oriented specimens of a single-crystal nickel-base superalloy', *Scr. Mater.*, 1999, **40**, (4), 389–395.
35. W. Österle, D. Bettge, B. Fedelich and H. Klingelhöffer: 'Modelling the orientation and direction dependence of the critical resolved shear stress of nickel-base superalloy single crystals', *Acta Mater.*, 2000, **48**, (3), 689–700.
36. L. Meric, P. Poubanne and G. Cailletaud: 'Single crystal modeling for structural calculations: part 1-model presentation', *J. Eng. Mater. Technol.*, 1990, **113**, (1), 162–170.
37. T. Tinga, W. A. M. Brekelmans and M. G. D. Geers: 'Cube slip and non-Schmid effects in single crystal Ni-base superalloys', *Modell. Simul. Mater. Sci. Eng.*, 2010, **18**, (1), 015005.
38. J. Wang, W. Guo, Y. Su, P. Zhou and K. Yuan: 'Anomalous behaviors of a single-crystal nickel-base superalloy over a wide range of temperatures and strain rates', *Mech. Mater.*, 2016, **94**, 79–90.
39. S. Ghosh, G. Weber and S. Keshavarz: 'Multiscale modeling of polycrystalline nickel-based superalloys accounting for subgrain microstructures', *Mech. Res. Commun.*, 2015. doi:http://dx.doi.org/10.1016/j.mechrescom.2015.12.001
40. M. A. Groeber and M. A. Jackson: 'DREAM.3D: a digital representation environment for the analysis of microstructure in 3D', *Integr. Mater. Manuf. Innov.*, 2014, **3**, (5), 1–17.
41. Simulation Modeling Suite. Simmetrix, 2015. Available at: http://www.simmetrix.com/.
42. J. Cheng, A. Shahba and S. Ghosh: 'Stabilized tetrahedral elements for crystal plasticity finite element analysis overcoming volumetric locking', *Comput. Mech.*, 2016, **57**, (5), 733–753.